THE JOURNAL OF PHYSICAL CHEMISTRY B

Article

pubs.acs.org/JPCB

Segregated Ice Growth in a Suspension of Colloidal Particles

Julia M. H. Schollick,[†] Robert W. Style,[‡] Arran Curran,[†] John S. Wettlaufer,[‡,§,∥] Eric R. Dufresne,[§,⊥] Patrick B. Warren,[#] Krassimir P. Velikov,[◊] Roel P. A. Dullens,[†] and Dirk G. A. L. Aarts*[,†]

[†]Department of Chemistry, Physical and Theoretical Chemistry Laboratory, University of Oxford, Oxford OX1 3QZ, United Kingdom

[‡]Mathematical Institute, University of Oxford, Oxford OX2 6GG, United Kingdom

[§]Yale University, New Haven, Connecticut 06520, United States

[∥]Nordita, Royal Institute of Technology and Stockholm University, SE-10691 Stockholm, Sweden

[⊥]ETH Zürich, CH-8093 Zürich, Switzerland

[#]Unilever R&D Port Sunlight, Wirral CH63 3JW, United Kingdom

[◊]Soft Condensed Matter, Debye Institute for Nanomaterials Science, Utrecht University, Princetonplein 5, 3584 CC Utrecht, The Netherlands

ABSTRACT: We study the freezing of a dispersion of colloidal silica particles in water, focusing on the formation of segregated ice in the form of ice lenses. Local temperature measurements in combination with video microscopy give insight into the rich variety of factors that control ice lens formation. We observe the initiation of the lenses, their growth morphology, and their final thickness and spacing over a range of conditions, in particular the effect of the particle packing and the cooling rate. We find that increasing the particle density drastically reduces the thickness of lenses but has little effect on the lens spacing. Therefore, the fraction of segregated ice formed reduces. The effect of the cooling rate, which is the product of the temperature gradient and the pulling speed across the temperature gradient, depends on which parameter is varied. A larger temperature gradient causes ice lenses to be initiated more frequently, while a lower pulling speed allows for more time for ice lenses to grow: both increase the fraction of segregated ice. Surprisingly, we find that the growth rate of a lens does not depend on its undercooling. Finally, we have indications of pore ice in front of the warmest ice lens, which has important consequences for the interpretation of the measured trends. Our findings are relevant for ice segregation occurring in a wide range of situations, ranging from model lab experiments and theories to geological and industrial processes, like frost heave and frozen food production.

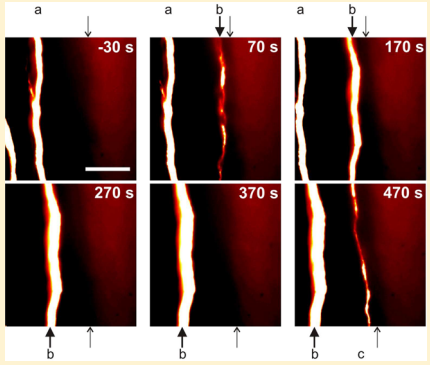

1. INTRODUCTION

Ice segregation is of key importance in determining the microstructure and bulk properties of materials in many different fields. Notably, it occurs in cold regions where soils and rocks are often damaged by the formation of bands of segregated (particle-free) ice lenses—a process called "frost heave". Processes that involve faster cooling rates also experience ice segregation. Freeze casting uses ice growth in particle suspensions to form porous ceramics, with controlled, anisotropic microstructure.[1−4] During the freezing of foods, the partitioning of colloidal scale particles from ice affects their texture and rheological properties.[5,6] In biology, ice segregation can cause disruption during the cryopreservation of biological matter[7,8] or in protein crystal annealing.[9]

Segregated ice growth is complicated, as evidenced by the wide community actively working to understand the physics that underlies this process (see, e.g., refs 10 and 11 for reviews specifically on frost heave). This is compounded by the fact that experiments on soils and engineering materials are hard to interpret, due to their heterogeneity and polydispersity. Thus, it is necessary to work with model systems, such as suspensions of colloidal particles, to carefully control the freezing process. Previous work has shown that, under slow freezing, ice growth in such media is determined by a number of factors. In particular, cooling rate[12] and particle size[13] both play a role in determining the final structures, due to their effect on the interaction of the particle with the moving ice interface,[14] and the effect curvature has on freezing, i.e., the Gibbs−Thomson effect.[15]

Here, we systematically study the process of ice lens growth in a simple model system using a directional solidification method (adapted from refs 16 and 17), which gives a fixed, well-defined rate of cooling. We freeze a suspension of colloidal silica particles in water unidirectionally. Our setup allows for microscopic inspection of the freezing process, measuring the initiation and evolution of the lenses under a range of

Received: January 22, 2016
Revised: March 26, 2016
Published: April 5, 2016

DOI: 10.1021/acs.jpcb.6b00742
J. Phys. Chem. B 2016, 120, 3941−3949

conditions. We focus on varying several factors, which are thought to affect ice lens formation but which have not yet been fully scrutinized in experiment: (i) the particle packing in the colloidal suspension and (ii) the cooling rate, as controlled separately by both the temperature gradient and the speed of sample motion across the gradient.

We start by describing the experimental methods in section 2. In section 3, we present our results: the general case (section 3.1) and the effect of changing the conditions (section 3.2). We discuss our results in section 4 and conclude in section 5.

2. EXPERIMENTAL METHODS

A directional solidification apparatus was used to observe the formation of segregated ice by freezing a thermally one-dimensional suspension of silica particles. A sample was pulled across a temperature gradient, G, at a fixed pulling speed, V, where both could be independently controlled. A diagram of the setup is shown in Figure 1.

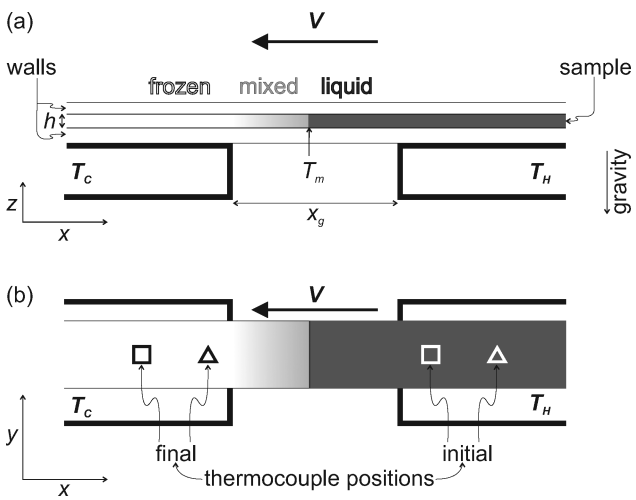

Figure 1. Schematics of the experimental setup (not to scale). The sample is placed on two temperature-controlled plates, at temperatures T_C and T_H, where T_m, the melting temperature of pure bulk water, is between the plates. The positive direction of the velocity of the motor, V, is shown. (a) The sample is contained within two glass walls and has depth h. The phases of the sample are shown above their corresponding x position, and the length of the gap between the plates, x_g, is also shown. (b) Initial and final positions of two thermocouples, represented by square and triangle symbols, are shown. The thermocouples are placed inside the sample and measure temperature as a function of position as they move with velocity V.

2.1. Sample Cell. The cell was prepared by gluing (UV glue NOA 81 with 60 s cure) two glass slides together with two glass slide "spacers" in between. All glass was washed with ethanol and then plasma cleaned for 1 min. The internal volume of the cell was $45 \times 12 \times 0.28$ mm^3 (length $l \times$ width $w \times$ depth h). The l and w dimensions of the cells could vary by a few millimeters and h by up to 0.02 mm. The area ($l \times w$) was not thought to affect the ice lens formation, as $l,w \gg h$.

2.2. Colloidal Model System. The silica particles were obtained as a powder from JGC Catalysts and Chemicals. They were polydisperse, with a documented average diameter of ~1.5 μm (with 90% particles ranging from 1−3 μm in size). Particle suspensions were made up with solutions of ultrapure water at two different initial particle volume fractions, $\phi_{p,i}$ = 0.31 and 0.41, in order to study the effect of particle packing, with initial concentrations determined by mass. The particles were washed with water 3 times by repeated centrifugation and redispersion. The suspension was dispersed by ultrasonic pulsation before being pipetted into the sample cell. The top of the cell was left open during the course of the freezing step. The particles were charge stabilized and have a zeta potential of −40 ± 5 mV (Malvern Zetasizer Nano Z).

In some cases, the particles were packed by centrifugation. Values of acceleration between 39g and 435g were used, with g Earth's acceleration, for 30 min. The centrifugation step changed the initial packing of the particle suspension. The smallest acceleration produced a diffuse interface between a layer of colloidal suspension and nearly pure water, which was close to the top of the cell. With increasing acceleration, the interface moved down the cell and became sharper. A simple estimate for the effective packing fraction, ϕ_p, is given by $\phi_{p,i} \times l/l_c$, where l_c is the length of the suspension after centrifuging. In the samples we tested, ϕ_p was calculated to be between 0.32 and 0.68 for the lowest and highest acceleration.

2.3. Directional Freezing. The sample was pulled across a fixed temperature gradient at a constant velocity. A Linkam GS350 stage was employed, which uses electrical resistance heaters and a pump-controlled flow of liquid nitrogen to control the temperature of two plates. The temperature gradient was created by independently fixing the temperature of the plates, which were separated by a gap of length $x_g \approx 2$ mm. The temperatures of the cold and hot plates, T_C and T_H, were held such that $T_C < T_m < T_H$, where T_m is the melting temperature of pure bulk water. The sample was observed in the gap. A stepper motor held the sample cell in contact with the plates and moved it along the gradient, G, at a velocity, V, with 1 μm increments. The sample depth was small, so a constant temperature along the z direction was assumed.[17] The apparatus depicted in Figure 1 was contained within a sealed box to prevent the condensation of water vapor, which would hamper observations.

First, ice was nucleated by setting $T_C = -30$ °C and holding T_H at room temperature. Several millimeters of the suspension was therefore "prefrozen", with rapid unstable growth of large ice crystals. This created irreversible changes in ϕ_p,[18] and therefore, this region was discarded during analysis. After the nucleation event, a temperature gradient was established by setting the plate temperatures: $T_C = -2$ °C and $T_H = 0.5$ °C. The gradient was left to stabilize for a minimum of 15 min before the motor was started at a speed of $V = 1.5$ μm s^{-1}. The duration of the directional freezing period was about 3 h.

2.4. Microscopy and Image Analysis. The sample was illuminated from below using a home-built Köhler lens microscopy setup. An image of the sample was projected onto a CCD camera, which had a field of view spanning nearly the entire length of the gap between the two plates. The suspension could be observed at temperatures close to and including T_m. Movies were recorded for the duration of sample freezing, typically at one frame every 5 s. After an experiment, the whole frozen sample was imaged to see the final structure. In all images presented the samples were frozen from left to right.

The optical contrast between the areas of ice and the areas of particle suspension (frozen and unfrozen) was large. Therefore, a simple image analysis technique was employed, where a threshold brightness was set, above which ice in a lens was determined to be present. In all images presented, segregated ice is light in color, as light is transmitted from the source below

DOI: 10.1021/acs.jpcb.6b00742
J. Phys. Chem. B 2016, 120, 3941−3949

and the frozen particle suspension is dark. The average thickness (x dimension) of lenses was calculated by measuring the thickness of a lens along its width (y dimension) and then taking the mean thickness of all lenses along the length (l) of the cell. In addition, the growth of single lenses was also measured using the same method.

2.5. Temperature Measurements. A standpipe was used to measure temperature at a fixed point in the cell. A standpipe is a cell containing pure water, which is built in parallel to the sample cell that contains the suspension.[19] The standpipe cell experiences to the best approximation the same conditions as the sample cell. Therefore, the position of the ice−water interface at the temperature of bulk melting, T_m, can be compared to the positions of interfaces in the parallel suspension-containing cell. The standpipe cell was made using the method described in section 2.1 but by placing an extra glass slide spacer along the center of a cell to divide it into two discrete sections. To determine the effect of nonparticulate impurities on the bulk melting temperature, a sample cell containing the supernatant of the suspension was also frozen under the same conditions.

The actual temperature gradient, G, within the sample cell was measured using two thermocouples fixed at different initial positions along x inside the cell, as shown in Figure 1b. The cell used was different to those described in section 2.1 only in its larger depth, 1.1 mm, in order to accommodate the thermocouples. The two independent thermocouples are used to verify each other's measurement and to enhance the range of the sweep. However, we note that this makes the assumption of the one dimensionality of the temperature gradient less certain.

3. RESULTS

In all samples regions of segregated ice were formed during directional freezing. The process of ice lens formation is presented in detail in section 3.1, and in section 3.2 we show the effects of changing conditions.

3.1. Segregated Ice Formation. Figure 2a shows a typical example of the macroscopically formed patterns. We first discuss the dynamics of ice lens growth (section 3.1.1) and then the final structure of the frozen suspension (section 3.1.2).

3.1.1. Growth of Segregated Ice. The emergence of segregated ice lenses perpendicular to the temperature gradient was observed. A time series showing the formation and growth of a lens (labeled lens 9) is seen in Figure 2b. Once a region of segregated ice is initiated within the suspension, it spreads quickly along the width (the y direction) of the cell to form a lens.

This lens then grows in thickness (parallel to the temperature gradient) due to flow of water through the suspension toward the ice lens. The motor speed, V, is faster than the growth rate of the lens. Therefore, the growing lens is translated toward colder temperatures, and the particle suspension ahead of the lens, in the direction of freezing, is cooled below T_m. A new lens nucleates within the suspension ahead of the growing lens, in the direction of freezing, when a critical temperature is reached. In the final image in Figure 2b, a new lens (labeled lens 10) nucleates at almost the same relative position as the previous two lenses (8 and 9). As a consequence, regularly spaced lenses emerge.

The lens must initiate from existing interparticle ice, as homogeneous nucleation does not occur at the temperatures inside the cell.[22] It is therefore probable that ice exists at the point where the warmest lens nucleates. We indeed detect an

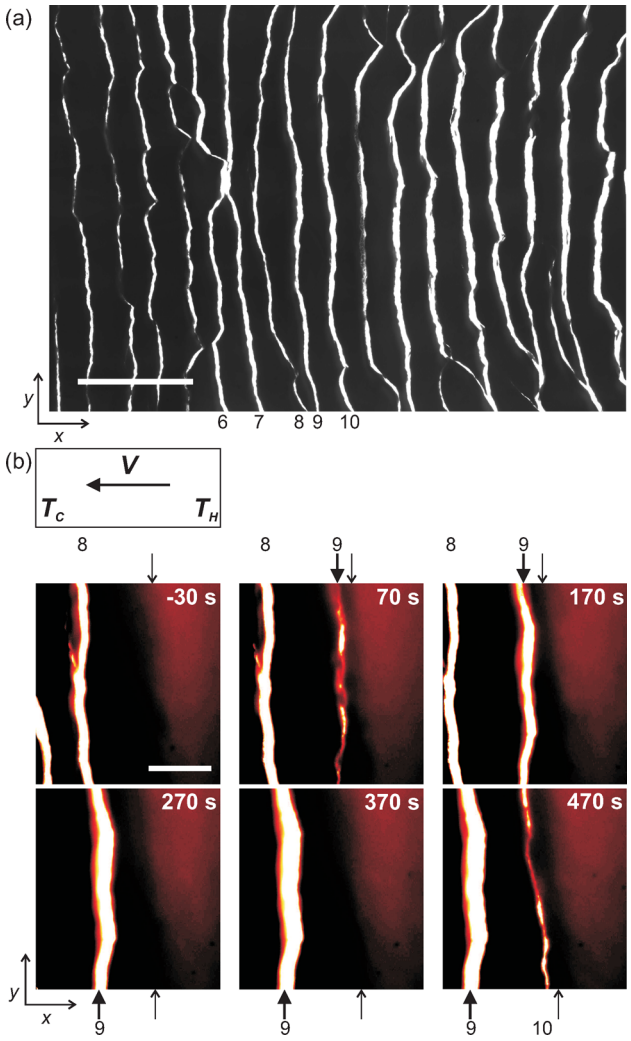

Figure 2. (a) Typical image of segregated ice in the form of ice lenses (labeled 6−10); segregated ice appears light, and frozen suspension appears dark. Scale bar denotes 2 mm. (b) Time series showing the nucleation of a lens; above the first image the relative positions of the cold and hot plates, T_C and T_H, and the direction of the pulling speed, V, is shown. The sample has moved across a distance of ($V \times$ time) in each subsequent frame. Thick arrows point toward the growing lens (9), and the surrounding lenses (8 and 10) are labeled. The image color has been processed using ImageJ (Fiji, "Red Hot" LUT)[20,21] to highlight the interface between the frozen suspension, which appears dark, and the unfrozen suspension, which appears red (lighter original color); thin arrows point toward this interface. The temperature range from left to right in each image is from −0.8 to −0.3 °C. Scale bar denotes 500 μm. The time is shown with respect to the approximate nucleation time of lens 9 at t = 0 s.

optically darker region (DR) of the particle suspension ahead of the warmest lens (see thin arrows in Figure 2b). The edge of the DR remains at the same position along the temperature gradient and thus is consistent with the idea that pore ice exists in the DR. If the temperature of the hot or cold plate is adjusted, we see movement of the DR edge corresponding to whether the overall temperature is increased/decreased. When water freezes, the refractive index (RI) changes from 1.33 to 1.31 while the silica particles have an RI of 1.54. The RI difference between the surrounding medium and the particle will therefore increase when ice is present. The enhanced refractive index difference on freezing (ice−particle) and also

DOI: 10.1021/acs.jpcb.6b00742
J. Phys. Chem. B 2016, 120, 3941−3949

the new ice−water RI difference will result in more scattering and therefore less transmission of light, hence rationalizing the DR. We note that because lens growth can compact the particles, this too can reduce the intensity of light transmission. However, if the extent of the DR would indeed be due to changes in the particle packing, we would expect an effect of particle concentration; in all cases (including the random close packing sample) in section 3.2.1, we see a DR.

In order to establish the temperature at which an ice lens nucleates, two methods were used (see section 2.5). First, the temperature was measured by two thermocouples as a function of position, x, as the cell traveled with velocity V. Second, use was made of a standpipe to determine the absolute temperature. The results are shown in Figure 3a and 3b. One cell contained just pure water and ice, and another cell contained the silica particles as well. The temperature gradient, G, is nearly constant between the plates. There is some heat transfer from the surroundings, but the two data sets overlap, and within error they are very nearly the same. The temperature gradient measurements are limited by both the precision of the thermocouples and the position determination. For the particle-containing cell, $G = 0.28$ K mm^{-1}; this value is used in all subsequent calculations.

In Figure 3b the position of the ice−water interface for pure water in the standpipe corresponds to $T = 0$ °C on the graph. The ice−water interface in the cell containing the supernatant of the particle suspension is displaced to colder temperatures, $x_{T_m} - x_{T_m(c \neq 0)} = 200 \pm 100$ μm, which corresponds to an undercooling of 60 ± 30 mK, using $\Delta T = G\Delta x$. Here, x_{T_m} and $x_{T_m(c \neq 0)}$ are the positions of the bulk melting temperature in the pure water and supernatant samples and c is the impurity concentration. Considering the colligative effect, where the cryoscopic constant for water is[23] $K_f \approx 1.9$ K M^{-1}, the undercooling of the supernatant relative to the pure water corresponds to an impurity concentration of ∼30 ± 14 mM, which we expect to be similar between different experiments. We note that the impurities are concentrated at the interface; therefore, the bulk impurity concentration will be lower than this value, see, e.g., ref 24.

The position of the dark region in the suspension contained in the standpipe cell, which was parallel to the pure water cell, has a larger undercooling at a displacement of $\Delta x_{DR} = x_{T_m} - x_{DR} = 1050 \pm 150$ μm, which corresponds to 300 ± 40 mK. Here, x_{DR} is the position of the edge of the dark region, which is also where the ice lenses nucleate. The position was measured by eye using the plot of pixel intensity as a guide (Figure 3b). The position is taken to be where there is a discontinuity corresponding to the change in light transmission before the intensity reduces due to the presence of the warm plate edge and microscope pinhole. Note that the DR is most easily established on a computer screen, where one can manipulate the image contrast. The implications of this undercooling will be discussed in section 4.

To quantify the growth process of ice lenses, the lens thickness, L_{th}, defined in Figure 4a, was measured as a function of time, t, see Figure 4b. The growth rate of a lens starts off being constant and only slows down as a new lens begins to form until it stops completely. Eventually it leaves the field of view. This basic pattern is repeated for consecutive lenses. The average growth rate of a lens during the constant growth period is 0.3 ± 0.03 μm s^{-1}.

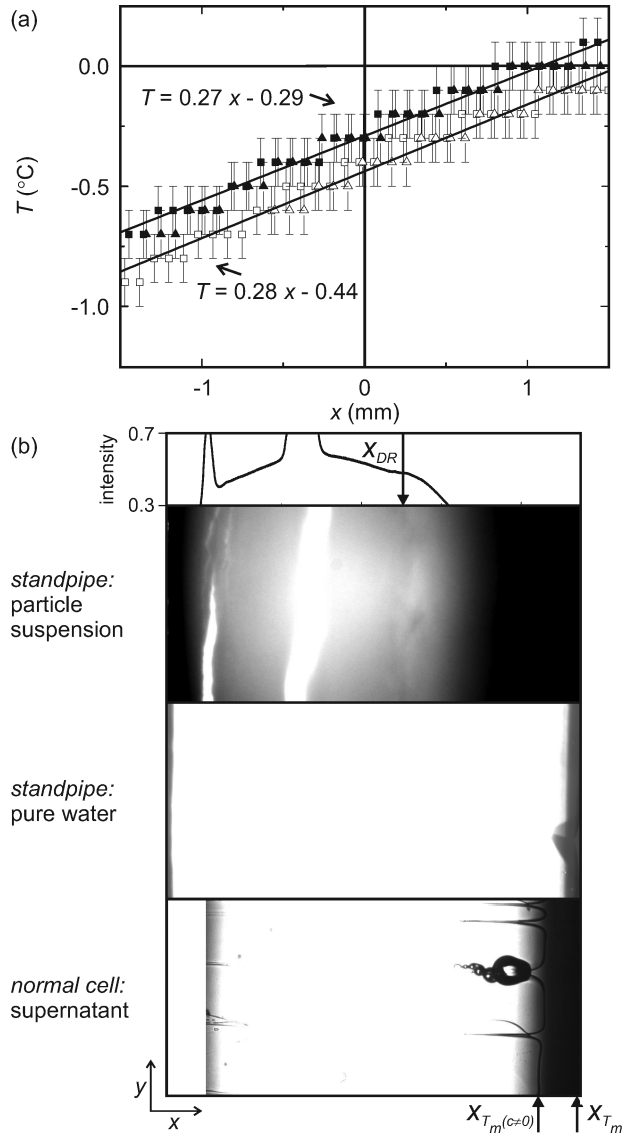

Figure 3. Methods of relating x positions to temperature. (a) Temperature, T, measured by the two thermocouples (square and triangle symbols) vs the distance along the cell, x, where $x = 0$ is the center between the plates. Two data sets are plotted: pure water + ice (filled symbols) and water and silica particles + ice (empty symbols), in which ice lenses form. Linear fits are plotted and labeled. (b) Three images placed at the corresponding x values of the graph (at the same scale), showing freezing in (top) a particle suspension, (center) pure water, and (bottom) the supernatant of the suspension. The ice−water interface, x_{T_m}, and the position of the edge of the dark region (also the lens nucleation position), x_{DR}, are marked by labeled arrows. x_{DR} is found by eye using a plot of the average pixel intensity over the y direction vs the x direction(shown above the image). The bottom two images are overexposed because a high light intensity was required to see the interface, which was beyond the warm plate edge. Note that gaseous impurities in the "normal" cell led to the formation of bubbles.

In order to probe the permeability of the frozen parts in the suspension and to investigate the ice lens growth rate after progressive cooling, the motor was stopped after the formation of several ice lenses in succession and directly after the nucleation of a new lens. We followed the growth of the lenses within the field of view, shown schematically in Figure 4a, and in Figure 4c, the lens thickness is plotted vs time. Lens 2 (L2) nucleates and grows linearly. Its growth then slows down as

DOI: 10.1021/acs.jpcb.6b00742
J. Phys. Chem. B 2016, 120, 3941−3949

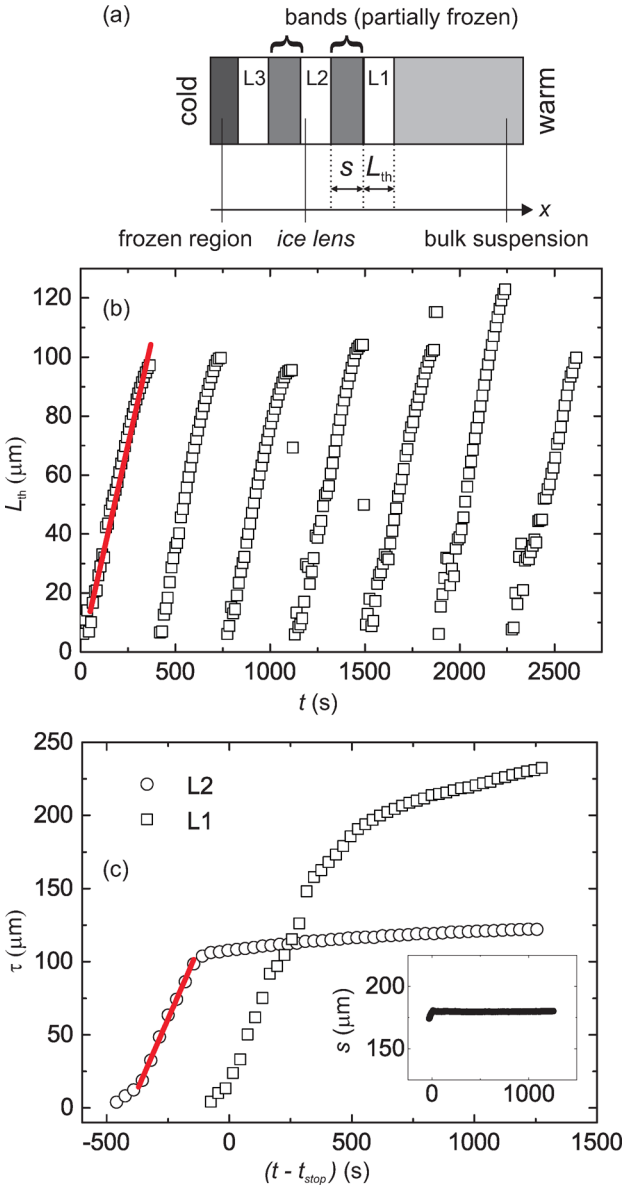

Figure 4. (a) Schematic diagram showing the final structure of the experiment, with definitions of the thickness, L_{th}, and spacing, s, of ice lenses, (b) mean thickness, L_{th}, of consecutive ice lenses plotted vs time, t, and (c) the mean thickness, L_{th}, of two lenses plotted vs the time after the motor has stopped ($t - t_{stop}$). (Inset) Spacing between lenses L1 and L2, s, vs ($t - t_{stop}$). (a and c) Before the motor stops, linear fits are used to measure the growth rate.

lens 1 (L1) forms, much the same as in Figure 4b. The motor is then stopped, and L1 continues to grow, eventually overtaking L2 in size. However, L2 continues to grow, as well albeit more slowly, while being colder than the newest ice lens. Because it grows from its warm edge, water must be supplied through the band between the lenses. Since the band, which is the region between the two lenses, stays of a roughly constant width (see the inset in Figure 4c), it suggests that either melting occurs at the cold edge of L1 or the unfrozen fraction in the band or both supply this water. The lenses that were colder than L2 (e.g., L3) did not grow after the motor stopped, indicating that ice was now completely blocking the pores in the colder band. L1 may continue to grow until the macroscopic ice is in equilibrium with the suspension, i.e., the warmest edge is close to the position of T_m.

3.1.2. Final Structures. The frozen suspension captures key features of frost heave, characterized by the average final thickness, L_{th}, and spacing, s, of the ice lenses (see Figure 4a). From this we calculate the ratio of ice lenses vs the frozen particle suspension, equal to L_{th}/s, which is a measure of the total heave of the suspension. For the example in Figure 2, the average thickness of the lenses was 90 ± 20 μm and the average spacing was 450 ± 35 μm, giving the proportion of ice lenses as 0.20. It is useful to compare these parameters after a change in experimental conditions: this is done in section 3.2. Finally, experiments where we deliberately doubled the height of the cell did not lead to any changes in the lens thickness or spacing. This strongly suggests that the third dimension (the z direction) does not play a significant role.

3.2. Effect of Changing Conditions. Final structures of ice lenses formed under different particle packing conditions and under different cooling rates are shown in Figure 5a−c.

3.2.1. Particle Packing. The influence of particle concentration is of key interest in the study of ice lens formation, affecting the permeability, ice fraction, and compressibility of the suspension. Here, we change the particle concentration either (a) by starting with different overall packing fractions or (b) by using different centrifugation speeds. Table 1 shows, with reference to each final structure presented in Figure 5a and 5b, the conditions under which they were prepared, including the initial particle concentration, $\phi_{p,i}$, the centrifugation acceleration, and the estimate for the final particle concentration, ϕ_p, directly before freezing was started. Note that method a provides a direct measure of ϕ_p. For method b, ϕ_p is based on an estimate as explained in section 2.2.

The plot in Figure 5d shows how the thickness, spacing of lenses, and average total heave change with packing conditions. Our results show that the spacing of ice lenses does not change significantly with ϕ_p. The lens thickness however varies considerably with ϕ_p and hence so too does L_{th}/s. For lower particle concentrations, the average lens thickness can be double that of a dense particle suspension, allowing heave to occur to a much greater extent. Importantly, the ice lenses formed with no centrifugation step (acceleration = 0) are less regular in thickness and shape than those formed with centrifugation, showing the role of heterogeneous packing. These lenses decrease in thickness over the course of the experiment (from left to right). As stated in section 2.2, the particles will be jammed into the cell by the centrifugation step, therefore producing a more regularly and more densely packed network of particles in a shorter suspension length. When the cell is placed perpendicular to gravity before the start of freezing, this particle network is less likely to vary over time due to sedimentation.

3.2.2. Growth Conditions. The growth conditions, controlled by the temperature gradient, G, and the pulling speed, V, are important parameters in ice lens formation and frost heave, since they can have a pronounced effect on the proportion of segregated ice formed in the particle suspension. Final structures are shown in Figure 5c, and Figure 5e shows how the thickness, spacing of lenses, and average total heave change with the product VG. In a single sample cell, the effect of changing V under a constant G was investigated (G = 0.28 K mm^{-1}, the first and third images), and in separate sample cells, G was changed, while V remained the same (V = 1.5 μm s^{-1}, the second and fourth images).

DOI: 10.1021/acs.jpcb.6b00742
J. Phys. Chem. B 2016, 120, 3941−3949

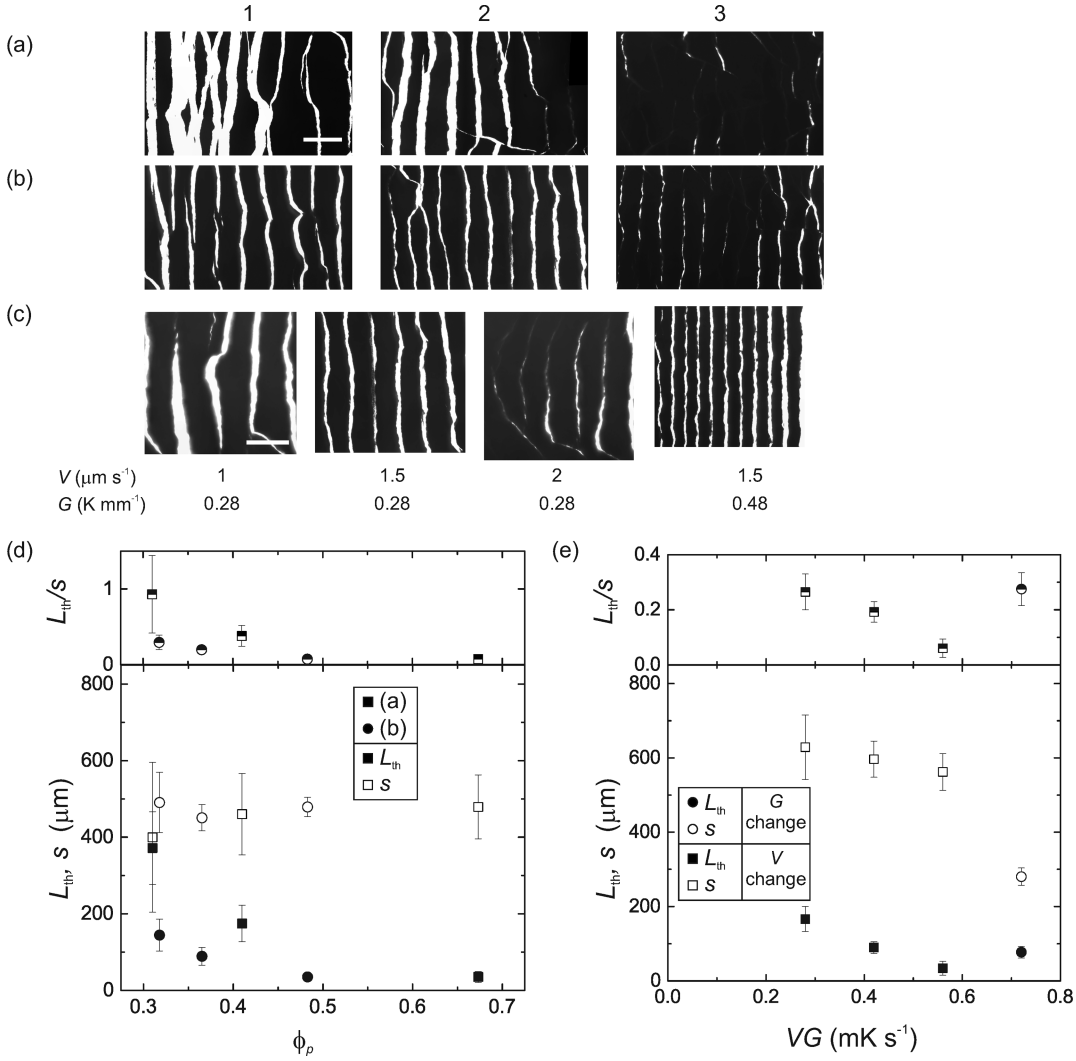

Figure 5. (a and b) Final structures of ice lenses formed under different particle packing conditions, as stated in Table 1. (c) Final structures of ice lenses formed under different cooling conditions. (d) Plot of the thickness, L_{th}, spacing, s, and L_{th}/s of ice lenses vs the estimated particle volume fraction, ϕ_p. (e) Plot of L_{th}, s, and L_{th}/s of ice lenses vs the cooling rate, VG. Scale bars all denote 1 mm.

Table 1. List of Experiments with Different Particle Packings[a]

Figure 5	$\phi_{p,i}$	acceleration	ϕ_p
		method a	
1	0.31		0.31
2	0.41		0.41
3	0.31	435*g*	0.68
		method b	
1	0.31	39*g*	0.32
2	0.31	156*g*	0.37
3	0.31	278*g*	0.48

[a]The ϕ_p after centrifugation is calculated as explained in section 2.2.

When V was increased, the average thickness of ice lenses reduced significantly and there was a slight reduction in the spacing. The final proportion of ice lenses (heave) decreased. The spacing only depends on the nucleation position of a new lens, relative to the edge of the previous one, and theory suggests this to be independent of V.[25] Therefore, the change in s can be accounted for mainly by the large change in L_{th}, and hence, L_{th}/s reflects the variation in L_{th}.

Upon increase of G (circle date point in Figure 5e, to be compared with second data point, at the same V), the lens thickness decreased slightly, but the decrease in spacing was more significant, and therefore the proportion of ice lenses, L_{th}/s, increased greatly. Here, the spacing changes significantly, because the initiation position of new lenses relative to the previous lens decreases with an increase of G, as expected in a steady temperature field.[25]

4. DISCUSSION

4.1. Lens Formation. Our system demonstrates the appearance of multiple ice lenses within a slowly freezing, closely packed porous suspension. The growth rate is between two extremes: ice rejecting particles indefinitely (primary frost heave) and the engulfment of particles by a fast freezing front. Within our system, both these regimes occur, within a mixed phase, where segregated ice grows as an ice lens by rejecting all particles. After further cooling, ice then grows into the suspension phase, in the pores between the particles. The ice effectively engulfs the particles within this phase until a new lens opens at a warmer temperature, and the old lens can become effectively frozen in place. However, at warm enough

DOI: 10.1021/acs.jpcb.6b00742
J. Phys. Chem. B 2016, 120, 3941−3949

temperatures we found that this colder, old lens can still grow, suggesting that a water supply still exists. Certain aspects of previous theories are observed in our system, and we will discuss our results in light of them below as well as highlighting any currently unexplained observations.

First, the presence of liquid water between frozen lenses and in the DR can be explained due to the solid/liquid interfacial curvature and/or colligative effects. The Gibbs−Thomson effect prevents ice from growing into the small pores, which allows water to continue to flow to a growing ice lens, even when it is below the bulk freezing temperature of water. This occurs because equilibrium between ice and water at a curved interface with temperature T requires that

$$\Delta T_{GT} = T - T_m = -\frac{T_m \gamma_{sl}}{L_m \rho_s}\kappa \quad (1)$$

where T_m = 273.15 K, the bulk melting temperature, $\gamma_{sl} = 3 \times 10^{-2}$ J m^{-2}, the solid−liquid (ice−water) surface tension, $L_m = 3.34 \times 10^5$ J kg^{-1}, the latent heat of fusion per kg of ice, ρ_s = 917 kg m^{-3}, the density of the solid, and a pore typically has a surface curvature of $\kappa \approx 2/R_p$, where R_p is the pore radius. Figure 6 shows how $\Delta x_F = x_{T_m} - x_F$, the positional shift

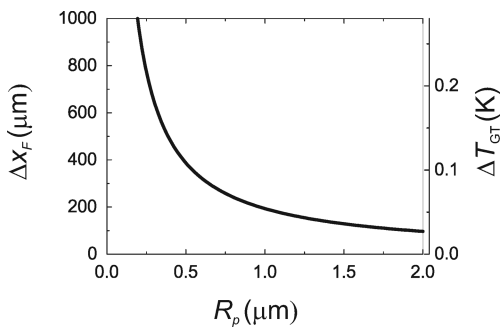

Figure 6. Plot of Δx_F (left-hand axis), which relates to the Gibbs−Thomson undercooling, ΔT_{GT}, by the temperature gradient G = 0.28 K mm^{-1} (right-hand axis), vs the radius of the pores, R_p.

corresponding to the change in melting temperature, varies with R_p. Here, x_F is the position up to which the pores are frozen and x_{T_m} is the position of the bulk melting temperature, and hence $\Delta x_F = \Delta T_{GT}/G$ according to eq 1.

Assuming that the pores are frozen up to the end of the DR, one can set $\Delta x_F = \Delta x_{DR}$, which is 850 ± 100 μm, taking the colligative effect into account (see Figure 3b). From this one can infer a pore radius of R_p = 0.23 μm. Furthermore, the ratio of pore radius to particle radius is R_p/R = 0.3. This is reasonable based on theoretical predictions for random close-packed spheres with a log−normal size distribution.[26,27] Alternatively, the measured x_{DR} may not be the limit of the presence of pore ice. For low particle packings, we would expect some pores to be much larger than the particle size, and therefore, a fraction of ice would be present very near the melting point (e.g., ref 28). However, our observations are consistent with the idea of having a reasonably sharp distinction between pore ice and pore water, and this measured interface position is consistent with theoretical predictions. The edge of the dark region is also where ice lenses nucleate, which agrees with frozen fringe theories. Models involving the presence of this frozen fringe, the region between a growing ice lens and the position where pores are frozen, successfully describe how intermittent ice lenses may form, e.g., refs 25 and 29−32, and a frozen fringe has been observed in other recent experiments using directional freezing apparatus.[27]

The fast propagation (Figure 2b) and subsequent wavy lens structure along the y direction (Figure 2a) can also be rationalized by the geometrical supercooling model proposed by Style et al.[28] They suggest a mechanism by which an ice-filled crack would propagate continuously along y, fracturing the suspension after its nucleation at the point with the largest geometrical supercooling, which is defined as the undercooling with respect to a spontaneous ice lens nucleation temperature. This supercooling is caused by a region of low permeability ahead of the first lens. The low permeability region could be caused by both spontaneous fluctuations in the concentration of particles ahead of the lens and/or ice presence in the pores. However, the ragged edge of a lens has other possible causes. For example, an inhomogeneity in particle packing along the y direction will result in a variation in the position of the edge of the frozen fringe and therefore the exact lens nucleation position.

4.2. Lens Growth. Our experiments show that the rate of ice lens growth is independent of the temperature of the ice lens growth surface. This surface is translated toward colder temperatures over time, and as the frozen fringe boundary is at a constant temperature throughout, the frozen fringe increases in thickness with time. It might seem plausible that as the fringe width increases, the ability to suck water toward the lens would decrease, therefore slowing the growth. Alternatively, if there was no fringe, it is expected that the water pressure next to the ice lens gradually decreases, according to the Clausius−Clapeyron equation, therefore causing an acceleration in the suction of water, see, e.g., ref 33. However, we see a period of constant growth. This is followed by an abrupt slowing down of the growth when a new ice lens is nucleated in front of it.

The permeability as a function of temperature may be measured by considering the change in growth rate in the stationary situation (Figure 4b and 4c). L1 continues to grow, after the motor is stopped (t = 0), its growth surface moving toward warmer temperatures, where the pore ice concentration will reduce. It slows down when the pressure gradient in the water diminishes. Water flux occurs across the bands between ice lenses: a warmer lens shrinks on its cold side, and a colder lens grows on its warm side, consistent with thermomolecular pressure-driven ice growth. This causes these interfaces to creep toward warmer temperatures. This behavior will occur until the permeability decreases such that pores are blocked by ice at low enough temperatures. Hence, our observation that at least one colder lens grows (Figure 4c), with the spacing between it and the warmer lens remaining constant, shows the importance of permeability in ice lens growth. This shows that segregated ice can evolve beyond dynamic cooling, therefore leading to further disruption of the particle suspension.

4.3. Changing the Particle Packing and Growth Conditions. The experimental results presented in Figure 5a, 5b, and 5d show that the particle packing is a key parameter in frost heave. Our observations show that ice lens formation occurs across a range of different packing fractions and furthermore that the particle packing has an effect on the growth rate of a lens. Some models of ice lens formation and frost heave take into account the effects of particle packing.[34,35] Though the effect of spacial inhomogeneity in the particle packing is a challenging problem not captured by most theories, some models simply fix the particle volume fraction, see, e.g.,

DOI: 10.1021/acs.jpcb.6b00742
J. Phys. Chem. B 2016, 120, 3941−3949

ref 30. Several factors may explain the reduction in thickness of ice lenses with increase in particle volume fraction. First, when particles are more closely packed, the suspension is less compressible and the ice lens will not be able to rupture the matrix. Second, the permeability of the suspension will be affected by the change in ϕ_p, reducing as a function of volume fraction. This reduction will cause the water flux toward the ice lens to slow down, resulting in thinner ice lenses. Third, a more concentrated particle suspension will mean there will be less water in the vicinity of the ice lens and therefore a smaller supply to the growing lens. Further experimental or theoretical work is required to determine the relative importance of these effects.

Figure 5b shows that increasing the time spent by the suspension at each temperature leads to an increase in lens thickness but does not affect the spacing. This is in agreement with other experiments, see, e.g., refs 27 and 36. The effect of temperature gradient on our system is also clear from Figure 5b. The spacing changes with frozen fringe thickness, which will depend on the temperature gradient. The thickness of ice lenses can change by either the time allowed for the ice lens to grow (changing V) or the frozen fringe thickness (changing G). If the frozen fringe is thicker, the suction of water toward the growing surface of the lens will be smaller. We here show that the individual terms control the ice lens formation, and the data does not collapse (Figure 5e). Our results are qualitatively consistent with the theory of Rempel et al.[25] and the experiments of Taber on clay,[37] where soil was frozen in an undefined temperature gradient, but the gradient could be inferred. The most frequent scenario in natural or industrial settings will be a change in temperature gradient, since most situations involve cooling by lowering the temperature from one end. Our experiments have shown that the change in heave in this case is significant.

5. CONCLUSIONS

We performed a series of experiments to observe segregated ice growth in the freezing of particle suspensions as a model for frost heave. Our results are relevant to many fields in which ice segregation is a significant issue: from the manufacture of frozen foods to the preservation of biotissue as well as in freezing soils. We find that regularly spaced ice lenses nucleate at a temperature where ice is likely to be present in the pores between the particles, and they grow at a rate which is independent of the undercooling.

We have shown that several factors are important in determining lens structures. In particular, variations in particle packing density strongly affect the final thickness of a lens and consequently the heave of the suspension. This will have implications for situations where changes in packing can occur over time, such as in cyclical processes like frost heave occurring in periglacial ground. Ice segregation itself causes regions of low and high particle concentrations in a suspension. Upon melting, this suspension will be more susceptible to ice lens growth in the less concentrated regions, therefore reinforcing the pattern formation process. Our model system also demonstrates some theoretically expected properties of lens formation, such as the changes in thickness and spacing of lenses upon a decrease in cooling rate and the crack-like propagation of a lens. This indicates a strong practical need to control these effects for an industrial process that include a particle suspension freezing step.

Finally, we have shown that suspensions containing colder ice lenses are not completely frozen and water can still flow through it. This raises the possibility that a particle suspension need not be progressively cooled for it to be influenced by ice lens growth. Certain factors described in this paper, such as the effect of many of the spatiotemporal variations in particle concentrations, have not yet been accounted for in theories on frost heave, and we hope our experimental data may stimulate further theoretical work along these lines.

■ AUTHOR INFORMATION

Corresponding Author

*E-mail: dirk.aarts@chem.ox.ac.uk.

Notes

The authors declare the following competing financial interest(s): P.B.W. holds equity (> $10k) in Unilever PLC. All other authors declare no competing financial interest.

■ ACKNOWLEDGMENTS

J.M.H.S. acknowledges EPSRC and Unilever for financial support. J.S.W. acknowledges Swedish Research Council Grant No. 638-2013-9243 and a Royal Society Wolfson Research Merit Award. We thank Stephen S. L. Peppin for many useful discussions.

■ REFERENCES

(1) Deville, S.; Saiz, E.; Nalla, R. K.; Tomsia, A. P. Freezing as a Path to Build Complex Composites. *Science* **2006**, *311*, 515−518.
(2) Zhang, H.; Cooper, A. I. Aligned Porous Structures by Directional Freezing. *Adv. Mater.* **2007**, *19*, 1529−1533.
(3) Deville, S.; Maire, E.; Bernard-Granger, G.; Lasalle, A.; Bogner, A.; Gauthier, C.; Leloup, J.; Guizard, C. Metastable and Unstable Cellular Solidification of Colloidal Suspensions. *Nat. Mater.* **2009**, *8*, 966−972.
(4) Elliott, J. A. W.; Peppin, S. S. L. Particle Trapping and Banding in Rapid Colloidal Solidification. *Phys. Rev. Lett.* **2011**, *107*, 168301.
(5) Mashl, S. J.; Flores, R. A.; Trivedi, R. Dynamics of Solidification in 2% Corn Starch-Water Mixtures: Effect of Variations in Freezing Rate on Product Homogeneity. *J. Food Sci.* **1996**, *61*, 760−765.
(6) Petzold, G.; Aguilera, J. M. Ice Morphology: Fundamentals and Technological Applications in Foods. *Food Biophys.* **2009**, *4*, 378−396.
(7) Hubel, A.; Darr, T. B.; Chang, A.; Dantzig, J. Cell Partitioning During the Directional Solidification of Trehalose Solutions. *Cryobiology* **2007**, *55*, 182−188.
(8) Deller, R. C.; Vatish, M.; Mitchell, D. A.; Gibson, M. I. Synthetic Polymers Enable Non-Vitreous Cellular Cryopreservation by Reducing Ice Crystal Growth During Thawing. *Nat. Commun.* **2014**, *5*, 3244.
(9) Garman, E. Cool Data: Quantity AND Quality. *Acta Crystallogr., Sect. D: Biol. Crystallogr.* **1999**, *55*, 1641−1653.
(10) Rempel, A. Frost heave. *J. Glaciol.* **2010**, *56*, 1122−1128.
(11) Peppin, S. S. L.; Style, R. W. The Physics of Frost Heave and Ice-Lens Growth. *Vadose Zone J.* **2013**, *12*, 0.
(12) Watanabe, K. Relationship Between Growth Rate and Supercooling in the Formation of Ice Lenses in a Glass Powder. *J. Cryst. Growth* **2002**, *237−239*, 2194−2198.
(13) Saruya, T.; Kurita, K.; Rempel, A. W. Experimental Constraints on the Kinetics of Ice Lens Initiation and Growth. *Phys. Rev. E* **2013**, *87*, 032404.
(14) Uhlmann, D. R.; Chalmers, B.; Jackson, K. A. Interaction Between Particles and a Solid-Liquid Interface. *J. Appl. Phys.* **1964**, *35*, 2986.
(15) Saruya, T.; Rempel, A.; Kurita, K. Hydrodynamic Transitions with Changing Particle Size That Control Ice Lens Growth. *J. Phys. Chem. B* **2014**, *118*, 13420−13426.
(16) Flemings, M. C. Solidification Processing. *Metall. Trans. A* **1974**, *5*, 2121−2134.

DOI: 10.1021/acs.jpcb.6b00742
J. Phys. Chem. B 2016, 120, 3941−3949

(17) Rubinsky, B.; Lee, C.; Chaw, M. Experimental Observations and Theoretical Studies on Solidification Processes in Saline Solutions. *Exp. Therm. Fluid Sci.* **1993**, *6*, 157−167.
(18) Spannuth, M.; Mochrie, S. G. J.; Peppin, S. S. L.; Wettlaufer, J. S. Dynamics of Colloidal Particles in Ice. *J. Chem. Phys.* **2011**, *135*, 224706.
(19) Zhu, D.; Vilches, O. E.; Dash, J. G.; Sing, B.; Wettlaufer, J. S. Frost Heave in Argon. *Phys. Rev. Lett.* **2000**, *85*, 4908−4911.
(20) Schneider, C. A.; Rasband, W. S.; Eliceiri, K. W. NIH Image to ImageJ: 25 years of image analysis. *Nat. Methods* **2012**, *9*, 671−675.
(21) Schindelin, J.; et al. Fiji: an Open-Source Platform for Biological-Image Analysis. *Nat. Methods* **2012**, *9*, 676−682.
(22) Angell, C. A. Supercooled Water. *Annu. Rev. Phys. Chem.* **1983**, *34*, 593−630.
(23) Aylward, G. H.; Findlay, T. J. V. *SI Chemical Data*; John Wiley & Sons: New York, 2002.
(24) You, J.; Wang, L.; Wang, Z.; Li, J.; Wang, J.; Lin, X.; Huang, W. Interfacial Undercooling in the Solidification of Colloidal Suspensions. *Rev. Sci. Instrum.* **2015**, *86*, 084901.
(25) Rempel, A. W.; Wettlaufer, J. S.; Worster, M. G. Premelting Dynamics in a Continuum Model of Frost Heave. *J. Fluid Mech.* **1999**, *498*, 227−244.
(26) Nolan, G. T.; Kavanagh, P. E. The Size Distribution of Interstices in Random Packings of Spheres. *Powder Technol.* **1994**, *78*, 231−238.
(27) Anderson, A. M.; Worster, M. G. Periodic Ice Banding in Freezing Colloidal Dispersions. *Langmuir* **2012**, *28*, 16512−16523.
(28) Style, R. W.; Peppin, S. S. L.; Cocks, A. C. F.; Wettlaufer, J. S. Ice-Lens Formation and Geometrical Supercooling in Soils and Other Colloidal Materials. *Phys. Rev. E* **2011**, *84*, 1−12.
(29) Gilpin, R. R. A Model for the Prediction of Ice Lensing and Frost Heave in Soils. *Water Resour. Res.* **1980**, *16*, 918−930.
(30) Konrad, J.; Morgenstern, N. R. A Mechanistic Theory of Ice Lens Formation in Fine-Grained Soils. *Can. Geotech. J.* **1980**, *17*, 473−486.
(31) Fowler, A. C.; Krantz, W. B. A Generalized Secondary Frost Heave Model. *SIAM J. Appl. Math.* **1994**, *54*, 1650−1675.
(32) Konrad, J.-M.; Shen, M. 2-D Frost Action Modeling Using the Segregation Potential of Soils. *Cold Reg. Sci. Technol.* **1996**, *24*, 263−278.
(33) Style, R. W.; Peppin, S. S. L. The Kinetics of Ice-Lens Growth in Porous Media. *J. Fluid Mech.* **2012**, *692*, 482−498.
(34) Peppin, S. S. L.; Wettlaufer, J. S.; Worster, M. G. Experimental Verification of Morphological Instability in Freezing Aqueous Colloidal Suspensions. *Phys. Rev. Lett.* **2008**, *100*, 238302.
(35) Peppin, S. S. L.; Majumdar, A.; Wettlaufer, J. S. Morphological Instability of a Non-Equilibrium Ice-Colloid Interface. *Proc. R. Soc. London, Ser. A* **2010**, *466*, 177−194.
(36) Watanabe, K.; Mizoguchi, M. Ice Configuration Near a Growing Ice Lens in a Freezing Porous Medium Consisting of Micro Glass Particles. *J. Cryst. Growth* **2000**, *213*, 135−140.
(37) Taber, S. The Mechanics of Frost Heaving. *J. Geol.* **1930**, *38*, 303−317.

DOI: 10.1021/acs.jpcb.6b00742
J. Phys. Chem. B 2016, 120, 3941−3949